FFI-RAPPORT

17/16257

Turbulent Boundary-Layer Simulations

comparison with experiments

–
Espen Åkervik

Turbulent Boundary-Layer Simulations

comparison with experiments

Espen Åkervik

Norwegian Defence Research Establishment (FFI) 5 October 2017

Keywords

Simulering
Turbulent strømning
Fluidmekanikk

FFI-rapport
FFI-RAPPORT 17/16257

Project number
1311,394801

ISBN
P: 978-82-464-2966-3
E: 978-82-464-2967-0

Approved by
Anders Helgeland, *Research Manager*
Janet M. Blatny, *Director*

Summary

The turbulent flow of gases and liquids plays an important role in a vast range of applications. Examples of this include atmospheric boundary layer flows, vehicles aerodynamics and internal combustion systems. From a societal security point of view, the dispersion of harmful substances in the form of aerosols and gases cannot be fully understood without taking turbulent transport into account. In the maritime sector, it is necessary to describe turbulent motion faithfully in order to be able to predict the hydrodynamic drag and to understand the noise generating mechanisms of vessels. Similarly, the prediction of aerodynamic drag, which is important to develop drag reducing designs on aircraft and vehicles, would be virtually impossible without detailed knowledge of turbulent flows.

In many cases it is possible to perform either full scale or model scale measurements to establish knowledge about the turbulent flows. Clearly, measurements have the advantage that there is no need to model the flow, and real-time data is possible to extract. On the other hand, the data is often collected in a noisy environment, and generally it is not possible to collect full space data.

The fast development of software and computer power has rendered computer simulation models based on solution of the Navier-Stokes equations an attractive tool to study turbulent flow phenomena. Recently, high fidelity techniques such as Large Eddy Simulation (LES) have become feasible for ever more complex problems. However, since LES methods require large computational resources, one needs to reduce the computational domain as much as possible. Due to this limitation, artificial boundary conditions at the upstream boundary of the computational domain are needed in order to describe the effect of the incoming flow.

This report presents LES results using a synthetic turbulence generator to supply artificial inflow conditions for two high Reynolds number turbulent boundary layer flows. In both cases, measurements are available for comparison. The motivation of this report is hence twofold. First, we aim to validate the performance of the Large Eddy Simulation model as a tool to study boundary layer flows. Second, we aim to quantify the performance of the synthetic turbulence generator.

The synthetic turbulence generator performs well for both flows. Although we find that high spatial resolution is needed to obtain a good measure of the skin friction, the large scale structures are captured even at relatively coarse resolution. This is important since the large scale structures are essential both in transport of aerosols and in flow noise generation.

Samandrag

Turbulent strømning av gassar og væsker spelar ei viktig rolle innanfor mange ulike bruksområde. Døme på dette er atmosfæriske grensesjikt, aero- og hydrodynamikken til fartøy og miksing i forbrenningsprosessar. I eit samfunnstryggleiksperspektiv er det til dømes vanskeleg å predikere spreiing av farlige emne i form av gassar og partiklar utan å ta omsyn til turbulent transport. I maritim sektor er det naudsynt å kunne skildre turbulente rørsler med stor grad av nøyaktigheit for å kunne berekne strømningsmotstand og strømningsindusert støy både på overflatefartøy, undervassbåtar og taua antennesystem. På same måte er designoptimering av fly og bilar for å redusere luftmotstand heilt avhengig av god kunnskap om turbulente strømningar.

I mange tilfelle er det mogleg å utføre enten fullskala eller modellskala målekampanjar for å få kunnskap om turbulens. Ein fordel med målingar er at ein ikkje treng å modellere strømninga, samtidig som det er mogleg å ekstrahere sanntidsdata. På den andre sida vert målingar ofte prega av støy, noko som gjer det vanskeleg å ekstrahere gode data. På grunn av avgrensingar ved måleteknikk er det generelt heller ikkje mogleg å samle inn alle data ein ønsker.

Den raske utviklinga i programvare og datakapasitet har medført at simuleringsmodellar basert på løysing av Navier-Stokes-likningar blir stadig meir eigna som verktøy for å studere turbulente strømningar. Nyleg har det vorte mogleg å bruke nøyaktige metodar, slik som Large Eddy-simulering (LES), på stadig meir komplekse problemstillingar. Sidan LES-metodar krev stor reknekraft, treng ein å avgrense berekningsområdet så mykje som mogleg. Ei slik avgrensing gjer at ein vert nøydd til å anta at den innkomande turbulente strømninga oppfører seg på ein spesiell måte. Ein set altså kunstige randkrav.

I denne rapporten har LES blitt brukt til å studere to turbulente grensesjikt med høge Reynoldstal. I begge tilfella har resultat frå vindtunnel vore tilgjengeleg for samanlikning, og i begge tilfella har ein syntetisk turbulensgenerator blitt brukt for å skape randvilkår for den innkomande strømninga.

Resultata viser at den syntetiske turbulensgeneratoren fungerer godt for begge strømningane. Sjølv om høg romleg oppløysing er naudsynt for å oppnå gode estimat på veggfriksjonen, vert dei store skalaene i turbulensen godt skildra, til og med for relativt låg oppløysing. Dette er viktig sidan desse strukturane er essensielle både i transport av aerosolar og i støygenerering.

Contents

1 Introduction

Turbulent flows are encountered in numerous industrial applications, atmospheric sciences and in everyday life. Turbulence is characterised by irregular chaotic motion, where large eddies, or whirls, create smaller eddies, which in turn create even smaller eddies. This process renders turbulence an efficient mixer of quantities such as heat, moisture, and aerosols. On one hand this leads to increased friction drag on vehicles, and therefore reduced performance, but on the other hand it enables efficient combustion processes. To be able to simulate turbulent motion is therefore essential both to understand and to create design improvements in a vast range of industrial applications.

In a turbulent flow, the size of the eddies range from the largest scale in the flow (i.e. that given by the geometry of the problem) down to a size of some millimetres or even micrometers. Generally, in order to simulate turbulent flows numerically, it is necessary to describe the full range of scales. This approach is known as Direct Numerical Simulation (DNS). The use of this method on most practical problems is almost impossible due to the high computational cost. Instead, the industry standard method builds on the so called Reynolds Averaging procedure, first formulated by Reynolds (1895), where only the mean flow is resolved, and the effect of the turbulent eddies on the mean flow is modelled. This class of methods is referred to as Reynolds Averaged Navier Stokes (RANS) methods. RANS methods has had significant success, especially in boundary layer dominated flows, such as the flow around air planes. However, the success has been limited in describing separated flows with vortex shedding, such as the wake behind buildings and vehicles, or buoyancy dominated flows, such as dense gas release. Large Eddy Simulation (LES) methods provide a means to accurately predict such flows. In LES, only the large eddies of the flow is resolved, whereas the action of the smaller eddies is modelled, thus rendering the method less costly than DNS in terms of computational resources. LES methods has proven very well suited to describe separated flows, however they are less efficient for boundary layer flows. This problem stems from the fact that close to walls, the large eddies are not that large. In fact their size is limited by the distance to the wall.

In the present work, LES of two boundary layer flows is performed, and the results are compared to experiments. It may seem contradictory to simulate boundary layer flows with a tool that is not primarily designed for such a task. However, even in flows dominated by vortex shedding, such as flow in urban environments or the wake behind vehicles, there will be interactions between the shed vortices and the incoming turbulent boundary layer flow. Therefore, it is essential to validate the performance of LES as a tool to study boundary layer flows. LES methods for boundary layer flows are in general computationally costly. Therefore, it is beneficial to reduce the size of the computational domain as much as possible. Boundary layers develop due to the presence of walls of objects that are placed in the flow. An example is the flat plate boundary layer flow, where a uniform flow impinges on a horizontal flat plate. Close to the leading edge the boundary layer is thin and supports only laminar flow states. Further downstream the boundary layer thickens and there is a transition to turbulence, followed by a region of fully developed turbulent flow regime. Most practical applications are in the fully developed turbulent regime and therefore it is mainly this regime that is of interest to simulate. However, if one is to limit the region of interest one arrives at the following question: What should the time dependent flow at the upstream boundary of the computational domain be? It is evident that knowing the mean flow is not sufficient, and neither is

the superposition of the mean flow and random perturbations, since turbulence is correlated both in time and space. So a follow up question may be: How much do we need to know about the turbulence that we have omitted to simulate?

For spatially homogeneous flows one has the possibility of imposing periodicity in the streamwise direction, thereby avoiding the problem of inflow conditions altogether. For spatially developing flows, which in industrial applications is the most common case, the simplest choice is to prescribe a laminar flow and introduce disturbances so that the flow naturally undergoes transition to turbulence. Disturbances may be introduced by tripping from obstacles or by volume forces mimicking the behaviour of these. This however, will in most cases yield a large computational domain, resulting in increased computational cost. In addition, it is not clear how well LES methods handle transition from laminar to turbulent flow regimes.

To introduce boundary conditions that mimic the behaviour of turbulent flows, there are according to Keating *et al.* (2004) three groups of methods: Recycling methods, precursor databases and synthetic turbulence. In addition, there is a class of methods built on systematic manipulation of experimental data.

Recycling methods, originally introduced by Spalart & Leonard (1985); Spalart (1986, 1988), simplified by Lund *et al.* (1998) and made more robust by Ferrante & Elghobashi (2004), use a modification of the periodic boundary conditions which takes into account the streamwise development of the flow. For the flat plate boundary layer flow Lund *et al.* (1998) extracted velocity data at a given downstream position. The data were rescaled both in inner coordinates (to match a desired friction velocity) and outer coordinates (to match a desired thickness and wake law). Although shown to give excellent results for the plate boundary layer flow, Keating *et al.* (2004) argues that there are drawbacks to the method; the most important being that the inlet must be placed in an equilibrium region (lack of generality), the fairly long fetch of the recycling region and the introduction of spurious periodicity (c.f. Spille-Kohoff & Kaltenbach, 2001).

Precursor databases are built by running separate simulations or experiments to build up the necessary information to be used as inflow. The precursor simulation is typically performed in a periodic domain, and a full transverse plane is stored at every time step. The velocity fields are then rescaled and used as input for the next simulation. The major drawback is that the precursor simulation may be as costly (in terms of computer power) as the simulation itself. In addition there may be considerable storage requirements when saving two-dimensional planes at every time step of a simulation. This method has been used with success in for instance Li *et al.* (2000), but little is known about the effects of significant rescaling when the target flow is far from the precursor flow.

The third class is that of synthetic turbulence. It is motivated by lack of generality in the two former classes of methods. In essence, the method is built on manipulation of random noise added to a mean velocity profile such that statistical moments and spectra resembles that of a turbulent flow. Several authors have pointed to the fact that the simplest choice, namely to add uncorrelated (in time and space) noise to mimic turbulent fluctuations, is a particularly bad choice that leads to immediate decay of turbulence (Druault *et al.*, 2004; Keating *et al.*, 2004). One method to obtain some spatial information is to create time series of velocity fluctuations by inverse Fourier transforms of known spectral densities, as was done in Le *et al.* (1997), where the amplitude of the Fourier modes were drawn randomly. The authors found that the missing phase

information led to a rapid decay of turbulence levels. In later works (Klein *et al.*, 2003; Batten *et al.*, 2004; di Mare *et al.*, 2006; Jarrin *et al.*, 2006), it was recognised that somehow the correlation in time and space should be considered. To further improve the results of the synthetic methods, Spille-Kohoff & Kaltenbach (2001) introduced forcing on successive downstream locations to penalise deviations from a prescribed Reynolds stress profile. In the review of Keating *et al.* (2004), the authors use a precursor periodic channel flow to generate a full data set in time and in the cross-flow plane to be used as inflow conditions for a spatially developing channel flow. They filter the full data and find that length scales larger than the integral length scale are the important ones to retain. In addition, the authors review the methods of Batten *et al.* (2004) and Spille-Kohoff & Kaltenbach (2001) and find that while typical synthetic methods require fairly long adaption region until a reasonable turbulent solution is obtained, the forcing method of Spille-Kohoff & Kaltenbach (2001) appears to be effective at reducing the adaption length.

In cases where sufficient experimental data is available, one may attempt to rebuild two-dimensional velocity fields with high temporal resolution directly from measurements. Particle image velocimetry (PIV) may provide two-dimensional snapshots of the flow with limited time resolution. On the other hand, good time resolution may be achieved by hot-wire probes, but at the cost of limited spatial resolution. In Perret *et al.* (2008), data from a rake of hot-wire probes is used to extract coherent structures from the flow by use of a proper orthogonal decomposition (POD). The authors build a reduced system of the flow using a Galerkin projection onto the basis of POD modes. The performance was limited by the need to retain only a few modes to keep the reduced system stable. In Druault *et al.* (2004), the authors devise a technique based on linear stochastic estimation. Their method relies on the knowledge of two-point correlations (POD modes) and high-fidelity time series at three points in space. The former can be obtained by a hot-wire rake or by PIV, whereas the latter may be obtained from hot-wire probes. A version of the method developed by Bonnet *et al.* (1994); Druault *et al.* (2004) has been successfully used at FFI to reproduce experimental results for a high Reynolds number turbulent boundary layer flow (see Wingstedt *et al.*, 2013). In that work, the coherent structures were extracted from PIV measurements and the time signals needed for the linear stochastic estimation were taken from a hot-wire rake.

In this report, a synthetic turbulence generator, similar to the method of Klein *et al.* (2003), is used to generate artificial inflow conditions based on limited experimental data for two different high Reynolds number boundary layer flows. The structure of the report is as follows. In Chapter 2, both the experimental and the numerical set up of the two flow cases are presented. In Chapter 3, the theoretical considerations are presented. The results are reported in Chapter 4. Concluding remarks are given in Chapter 5.

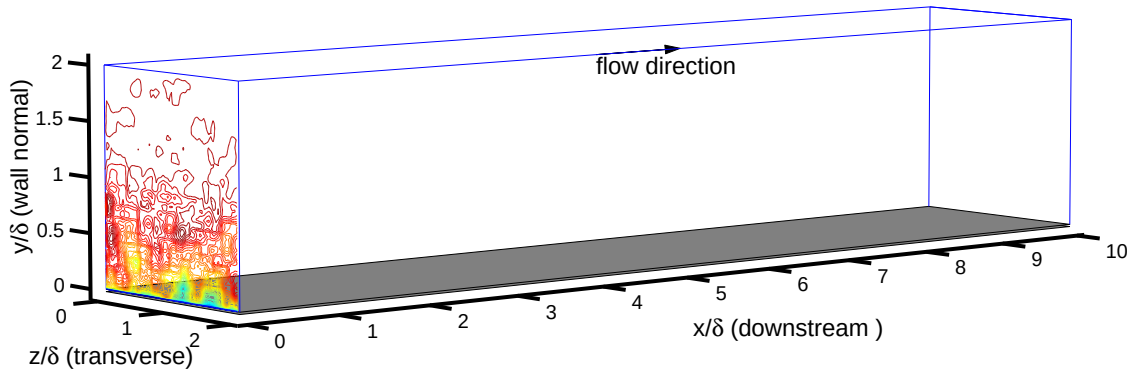

Figure 2.1 *Illustration of the computational box for boundary layer flows. All lengths in the illustration are normalised by the boundary layer height δ.*

2 Flow configurations

In this report, two different turbulent boundary layer flow configurations are considered. Figure 2.1 shows the basic setup. At the inflow a time varying synthetic velocity field is prescribed, defining a unidirectional freestream flow U_∞ flowing over a wall. Towards the wall, the flow is decelerated due to viscous shear forces, thereby defining a boundary layer of thickness δ. Since the imposed inflow boundary conditions are not true solutions to the Navier–Stokes equations, there will be an adaptation region some distance downstream of the inflow, where some disturbances are dampened, while others are amplified. Results from the simulations are compared to results obtained from wind tunnel experiments. Table 2.1 describes the relevant parameters defining the different cases. Case A was computed as a baseline flat plate boundary-layer flow to compare with turbulent flow over linear surface waves in the project FFI project "Maritime Boundary Layers". The simulation parameters are set to match experimental data from the WALLTURB project (Delville *et al.*, 2009). Case B is a boundary layer flow to be used as inflow data (precursor simulation) for dispersion modelling in the European Defence Agency (EDA) funded "MODITIC" project. Here, the numerical setup matches the setup of the EnFlo wind tunnel in Surrey. The computational grid used in each of the flows are given in Table 2.2 and the next sections describe the two experiments in more detail.

Table 2.1 *Setup for the different boundary layer simulations. Both cases are air flows (i.e. $\nu = 1.5 \times 10^{-5}\, m^2/s$). The viscous lengths, l^+, are defined based on experimental values of the friction velocity (see sections 2.1 and 2.2 for definitions).*

Case	U_∞ (m/s)	u_τ (m/s)	δ (m)	$Re_\delta = \frac{U_\infty \delta}{\nu}$	$l^+ = \nu/u_\tau$ (m)	$Re_\tau = \delta/l^+$
A	10	0.35	0.3	2.0×10^5	4.3×10^{-5}	7.0×10^3
B	1.068	0.055	1.0	7.12×10^4	2.6×10^{-4}	3.9×10^3

Table 2.2 *Grid sizing for the different cases. Cases A1 and A2 (see Table 2.1) use uniform spacing in the horizontal directions and geometric grid stretching in the wall normal direction. The grid spacing increases by a factor of $r = 1.069$ for each grid point away from the wall in case A1. The corresponding growth for A2 is $r = 1.044$. In Case B (see Table 2.1), three grids are stitched together. The finest grid is close to the wall, i.e. below $y/\delta = 0.02$. Between $y/\delta = 0.02$ and $y/\delta = 0.51$ a three times coarser grid is used. Above $y/\delta = 0.51$ an even three times coarser grid is used. This type of grid is referred to as a 1 to 3 split grid, or a boundary layer grid. The lower grid is squeezed in the wall normal directions, whereas the two upper grids have uniform spacing. Grid spacing nondimensionalised by viscous length is computed as $\Delta x^+ = \Delta x/l^+$, where l^+ is taken from Table 2.1.*

Case	Grid type	L_x/δ	L_z/δ	L_y/δ	$N \cdot 10^{-6}$	Δx^+	Δz^+	Δy^+_{min}	Δy^+_{max}
A1	Stretch wall normal	10	2	2	19.6	95	55	1	900
A2	Stretch wall normal	10	2	2	0.75	700	142	1	591
				0.02		16	16	7	7
B	1 to 3 split	8	1.5	0.49	10.7	47	47	47	47
				0.99		144	144	144	144

2.1 The WALLTURB high Reynolds number experiments

Figure 2.2 *The LML wind tunnel. (Picture taken from Stanislas* et al. *(2009*b*)).*

WALLTURB was a European Commission funded collaborative project that lasted for four years (2005-2009) involving 16 partners, where the aim was to gain more insight to near wall structures in high Reynolds number turbulence. The work consisted of wind tunnel experiments, Direct Numerical Simulation studies and turbulence modelling efforts. The experiments were performed in the large Laboratoire de Mécanique de Lille (LML) wind tunnel (see Figure 2.2). The test section is 20 m long with a cross section of $1 \times 2\,\text{m}^2$. Air with a kinematic viscosity of $\nu = 1.5 \times 10^{-5}\,\text{m}^2/\text{s}$ was driven through the tunnel at the two different freestream velocities

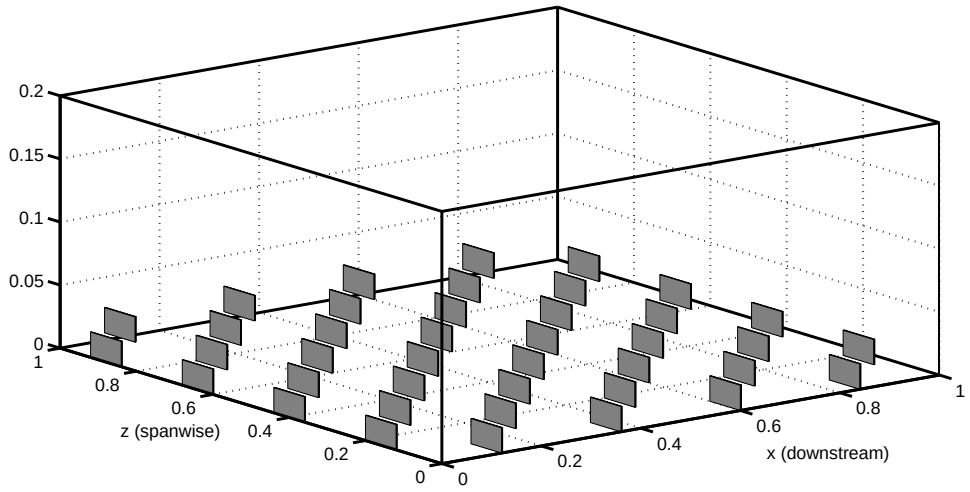

Figure 2.3 *Illustration of roughness elements in the EnFlo tunnel.*

of $U_\infty = 5\,\mathrm{m/s}$ and $U_\infty = 10\,\mathrm{m/s}$. In both cases, the boundary layer thickness was $\delta = 0.3\,\mathrm{m}$. Friction velocities obtained through the so called Clauser plotting procedure was $u_\tau = 0.18\,\mathrm{m/s}$ and $u_\tau = 0.35\,\mathrm{m/s}$, respectively. This yielded friction Reynolds number of $Re_\tau = 3600$ for the freestream velocity of 5 m/s and $Re_\tau = 7000$ for the freestream velocity of 10 m/s.

The tunnel was instrumented with a hot-wire rake consisting of 143 single wire probes distributed in the wall normal and spanwise plane with a wall normal extent of 306.6 mm and a spanwise extent of 280 mm. The lowest row of probes were located at $y = 0.3\,\mathrm{mm}$, corresponding to $y^+ = yu_\tau/\nu = 7.5$ for the lowest Reynolds number. The rationale behind the use of a large rake was to capture temporally well resolved velocity data with some spatial extent. The blockage effects present was addressed in Stanislas *et al.* (2009*a*). In addition, to complete the spatial information, two stereoscopic PIV systems were used. Based on the data from the stereo-graphic PIV system and the hot-wire rake data, Wingstedt *et al.* (2013) devised a method to combine the high spatial resolution of the PIV data with the high temporal resolution of the hot-wire data using Linear Stochastic Estimation (LSE).

2.2 The EnFlo urban dispersion experiments

Within the European Defence Agency (EDA) funded project "Modelling the dispersion of toxic industrial chemicals in urban environments" (MODITIC), experiments where performed in the EnFlo wind tunnel located at the Environmental Flow Research Centre in Surrey. The test section is 20 m long with a $3.5 \times 1.5\,\mathrm{m}^2$ cross section, and an air-speed range of 0.3 m/s to 4.5 m/s. The tunnel has capability of running stratified conditions. Vertical profiles of mean velocity and turbulent Reynolds stresses was measured for neutrally stratified conditions. The boundary layer is of depth $\delta = 1\,\mathrm{m}$ with a freestream velocity of $U_\infty = 1.068\,\mathrm{m/s}$. Data from the experiments were collected with a two-component Dantec Laser Doppler Anemometer (LDA) system.

The friction velocity was estimated from the mean shear stress over the lower 20% of the boundary layer, i.e.

$$u_\tau = \sqrt{(1/N)\sum_{i=1}^{N}\langle uv\rangle_i}, \quad \langle uv\rangle_i = \langle uv\rangle(y_i), \quad y_i = \{0.02, 0.026, \ldots, 0.2\}, \tag{2.1}$$

yielding a value of $u_\tau = 0.055$ m/s. The corresponding length scale was $l^+ = \nu/u_\tau = 2.7\times10^{-5}$ m, leading to a friction Reynolds number of $Re_\tau = \delta/l^+ = 3.6 \times 10^3$. Roughness elements of height $h/\delta = 0.02$ are placed at the lower wall. The elements have a downstream spacing of 0.12 m and a spanwise spacing of 0.08 m. There is an alternating shift between consecutive rows, so that every second row is at the same spanwise location, whereas the row in between is shifted a distance of 0.12 m in the spanwise direction (see Figure 2.3). The effective roughness length, found by curve fitting to a log profile, is $z_0/\delta = 8 \times 10^{-4}$. This corresponds to a roughness Reynolds number of $Re_{z_0} = Re_\tau\, z_0/\delta = 2.9$, which may be considered as fully rough conditions, i.e. the pressure drag created by the obstacles dominates the viscous effects at the wall (c.f. Ikeda & Durbin, 2007). Nevertheless, as will be described later, two simulations are performed; one where the boundary layer is assumed to be of smooth wall type and one where the exact roughness elements are introduced at the lower wall.

3 Theoretical considerations

3.1 Governing equations

Generally, the motion of fluids can be described by a set of conservation equations along with a number of constitutive relations describing the material properties of the fluid. We here consider incompressible Newtonian fluids for which the motion is governed by conservation of mass and momentum (Kundu *et al.*, 2012)

$$\begin{aligned} \nabla \cdot \mathbf{u} &= 0, \\ \rho \left(\partial_t \mathbf{u} + \mathbf{u} \cdot \nabla \mathbf{u} \right) &= \nabla \cdot \sigma, \end{aligned} \tag{3.1}$$

where $\mathbf{u} = \mathbf{u}(x, y, z, t)$ is the velocity vector in all three spatial directions, ρ is the density and σ the stress tensor. For Newtonian fluids, the constitutive relation, linking the flow gradients to the stresses, is expressed as

$$\sigma = -p\mathbf{I} + 2\mu\mathbf{s}. \tag{3.2}$$

Here, p is the pressure acting normal to any surface, μ is the dynamic viscosity and $\mathbf{s}$ is the strain rate tensor

$$\mathbf{s} = \frac{1}{2} \left(\nabla \mathbf{u} + (\nabla \mathbf{u})^T \right). \tag{3.3}$$

The set of equations (3.1) are referred to as the Navier–Stokes equations for incompressible Newtonian flow. The equations need suitable initial and boundary conditions to be solved. Later, the subject of inflow boundary conditions will be discussed in more detail.

3.2 Numerical modelling

The Navier–Stokes equations need to be solved numerically, since exact solutions only exist for very simplified problems. The presence of turbulence renders the direct numerical solution (DNS) difficult due to the large range of both spatial and temporal scales that need to be described. One possible method is to use a Large Eddy Simulation (LES) technique, where formally the equations are filtered to keep only the low frequency part of the spectrum, i.e. discarding the smallest scales in the problem (Sagaut, 2006). The filtering operation leads to extra unclosed advection terms. The resulting terms can be written as a tensor adding to the stress tensor in eq. (3.1)

$$\sigma = -p\mathbf{I} + 2\mu\mathbf{s} + \sigma_{\mathrm{SGS}}, \tag{3.4}$$

which describes the effect of the neglected small scale fluctuations on the resolved flow field. The task is now to model the tensor σ_{SGS} in terms of resolved variables. In the dynamic Smagorinsky sub-grid scale viscosity model, where the effect of the unresolved small scales are modelled as "viscous" effects, one writes

$$\sigma_{\mathrm{SGS}} = -2\nu_{\mathrm{SGS}}\mathbf{s}, \quad \text{with} \quad \nu_{\mathrm{SGS}} = \nu_{\mathrm{SGS}}(\mathbf{x}, t). \tag{3.5}$$

The sub-grid viscosity in the dynamic Smagorinsky model is computed from the resolved strain rate $\mathbf{s}$ and the grid size of the problem. Further details on LES theory and methodology, as well as the computational route to finding the eddy-viscosity, can be found in e.g. Pope (2000); Sagaut (2006).

In this report, we use a Finite Volume Method based LES solver developed at Cascade Technologies (Mahesh *et al.*, 2002; Ham & Iaccarino, 2004; Mahesh *et al.*, 2004; Ham *et al.*, 2006). It is second-order accurate in space and up to second order accurate in time, and a fractional step pressure correction method is applied to enforce divergence free solutions. Applications to turbulent problems at FFI using Large Eddy Simulation are found in Wingstedt *et al.* (2013); Rashid *et al.* (2011); Vik *et al.* (2015); Vartdal (2016); Wingstedt *et al.* (2016) and in the PhD thesis of Fossum (2015) and the papers therein.

3.3 Statistical measures

The resolved flow fields can be decomposed into mean and fluctuating parts, i.e. $\mathbf{u} = \mathbf{U} + \mathbf{u}'$, $p = P + p'$. Here, upper-case symbols ($\mathbf{U}$ and P) denote averaged fields, whereas lower-case prime symbols represent fluctuations around the mean. All averages reported in this work are averaged in time and spanwise (z) direction. For instance, for the velocity field we write

$$\mathbf{U}(x, y) = \langle \mathbf{u}(\mathbf{x}, t) \rangle = L_z^{-1} T_{\text{av}}^{-1} \int_0^{T_{\text{av}}} \int_0^{L_z} \mathbf{u}(\mathbf{x}, t) \mathrm{d}z \mathrm{d}t, \tag{3.6}$$

in which $\langle \cdot \rangle$ denotes the averaging operator. The Reynolds stresses are defined as

$$\mathbf{R}(x, y) = \langle \mathbf{u}'(\mathbf{x}, t) \mathbf{u}'(\mathbf{x}, t) \rangle = \begin{bmatrix} \langle u_1' u_1' \rangle & \langle u_1' u_2' \rangle & \langle u_1' u_3' \rangle \\ \langle u_2' u_1' \rangle & \langle u_2' u_2' \rangle & \langle u_2' u_3' \rangle \\ \langle u_3' u_1' \rangle & \langle u_3' u_2' \rangle & \langle u_3' u_3' \rangle \end{bmatrix}, \tag{3.7}$$

which is a symmetric, i.e. $\mathbf{R} = \mathbf{R}^T$, covariance matrix. The Reynolds stresses represent one-point one-time correlations, which provide local information on the statistics. To obtain information on the spatial structure of the flow the simplest statistical measure is the two-point one-time auto covariance (Pope, 2000)

$$\mathbf{R}(\mathbf{r}, x, y) = \langle \mathbf{u}'(\mathbf{x}, t) \mathbf{u}'(\mathbf{x} + \mathbf{r}, t) \rangle, \tag{3.8}$$

which for $\mathbf{r} = 0$ reduces to the standard one-point one-time correlations. The streamwise integral length scale may then be defined as

$$L_{11}(x, y) = \frac{1}{R_{11}(0, x, y)} \int_0^{\infty} R_{11}(r_x, x, y) \mathrm{d}r_x, \tag{3.9}$$

and the other directions are defined similarly. Two-time one-point statistics can be defined by introducing a time lag instead of a distance in Equation (3.8), i.e. $\mathbf{R}(\tau, x, y) = \langle \mathbf{u}'(\mathbf{x}, t) \mathbf{u}'(\mathbf{x}, t + \tau) \rangle$.

3.4 Synthetic inflow boundary conditions

Consider a rectangular box of size $L_x \times L_y \times L_z$ (see Figure 2.1). The mean flow is in the $x-$direction, with inflow at $x = 0$ and outflow at $x = L_x$. The wall is located at $y = 0$, and at $y = L_y$

the presence of the wall should not be felt. The z direction is a transverse homogeneous direction (with respect to the wall and the direction of the freestream) and can be treated as periodic. A requirement is that the length L_z should be sufficiently large to capture the relevant structures of the flow. For the flat plate boundary layer flow this corresponds to a few transverse integral length scales. At the lower wall, where $y = 0$, no-slip conditions are enforced. At the outflow boundary, $x = L_x$, an advective scheme is imposed, ensuring that structures propagate out of the domain with minimal reflections. Note that a couple of boundary layer thicknesses upstream of the outflow boundary, the results are usually affected by the boundary condition, and this region should be discarded from analyses. At the top of the computational domain ($y = L_y$) the task is to truncate the "infinite" domain in the wall normal direction. To accommodate a growing boundary layer in an incompressible flow, entrainment of fluid from above is needed. In the present work, we a apply a slip condition at the top. This effectively means that there is no entrainment of fluid. The boundary layer thickness can hence not be expected to develop correctly downstream. Instead, one can view the resulting flow field as a frozen downstream position with sufficient spatial extent for large scale turbulent structures to exist. Care has to be taken that the domain is sufficiently high to minimise the acceleration of the fluid.

The inflow boundary conditions at $x = 0$ is by far the most challenging to determine, since this requires knowledge about the incoming turbulent flow. When simulating a boundary layer flow using the Reynolds Averaged Navier-Stokes (RANS) equations only mean flow conditions, $U_i(y, z)$, are necessary to impose. However, when using Direct Numerical Simulation (DNS) or Large Eddy Simulation (LES), one needs to introduce also the time varying fluctuations $u_i'(y, z, t)$. These fluctuations $u_i'(y, z, t)$ should be prescribed in such a way that the flow downstream develops as fast as possible into a reasonable turbulent field without actually having to solve the full problem, i.e. without simulating the incoming turbulent flow. In the code from Cascade Technologies, a synthetic turbulence generator based on filtering of white noise in Fourier space is used. This method is similar to the method of Klein *et al.* (2003); di Mare *et al.* (2006). Recently, also a synthetic turbulence generator based on differential filtering of randomly generated signals in physical space was added to the code. However, in this report we only consider the former method.

4 Results

4.1 Recreating the flow in the WALLTURB LML tunnel

In the WALLTURB project, turbulent boundary layer flows were studied for a range of freestream velocities. We seek here to reproduce the flow with a freestream velocity of $U_\infty = 10\,\mathrm{m/s}$. For this case, the authors of Delville *et al.* (2009) report a boundary layer thickness of $\delta = 0.3\,\mathrm{m}$ and a friction velocity of $u_\tau = 0.35\,\mathrm{m/s}$, leading to a friction Reynolds number of $Re_\tau = U_\tau \delta/\nu = 7000$. Note that the exact determination of the friction velocity is in general challenging when analysing experimental results. However, in the present experiment, the three methods of Clauser plot, PIV and oil-film interferometry yielded very similar results. Hence, one can conclude that the obtained estimate of the friction velocity is rather good. The viscous length scale computed based on the friction velocity is $l^+ = \nu/u_\tau = 4.3 \times 10^{-5}\,\mathrm{m}$.

To generate suitable inflow boundary conditions, the mean and the Reynolds stress profiles are used in conjunction with the digital filter synthetic turbulence generator. There are two free parameters to be set; namely an estimate of the transverse integral length scale and an estimate of the streamwise integral time scale. In the PhD thesis of Tutkun (2008), the author gives estimates of these quantities for this specific flow, and finds that the transverse integral length scale grows monotonically from approximately $L_z^i/\delta = 0.02$ close to the wall to approximately $L_z^i/\delta = 0.15$ at the top of the boundary layer. The streamwise integral time scale increases from $T_x^i U_\infty/\delta = 0.15$ close to wall to $T_x^i U_\infty/\delta = 0.5$ at $y/\delta = 0.13$. Thereafter, it decreases to $T_x^i U_\infty/\delta = 0.3$ at the top of the boundary layer. Following Keating *et al.* (2004), who recommended to retain the largest length scales, we choose a slightly higher value of the transverse integral length scale of $L_z^i/\delta = 0.2$. The integral time scale is set to $T_x^i U_\infty/\delta = 0.2$, which is in the lower part of the range reported in Tutkun (2008). The influence of the choice of integral length and time scales will be discussed later.

Two computational grids are considered. The details of the computational grids are given in Table 2.2 as case A1 for the fine grid and A2 for the coarse grid. For case A1, the computational grid has dimensions $L_x \times L_y \times L_z = 10\delta \times 2\delta \times 2\delta$, whereas for case A2 the dimensions are $L_x \times L_y \times L_z = 10\delta \times 2\delta \times \delta$ The horizontal grid resolution for case A1 (A2) is $\Delta x^+ = 95\,(700)$, $\Delta z^+ = 55\,(142)$ in the streamwise and spanwise direction, respectively. In the wall normal direction, both case A1 and A2 use grid stretching with geometric growth from the wall to the top of the domain. In both cases the first grid point is located at $y^+ = 1$ (corresponding to $y/\delta = 1.42 \times 10^{-4}$). The geometric growth factor is $r = 1.069$ for case A1, and $r = 1.044$ for case A2. For case A1 this yields a grid spacing of $439\,l^+$ at the top of the boundary layer ($y/\delta = 1$) and $900\,l^+$ in the dynamically less import freestream at $y/\delta = 2$. It has been verified using the horizontal resolution as in case A2, by varying the wall normal resolution, that the relatively large vertical grid spacing used in case A1 in the wall normal direction at the top of the domain has no significant effect on the statistics. Simulations are performed in two stages. Initially a period of $TU_\infty/\delta = 50$ inertial times is simulated to achieve a statistically steady state of the flow variables, starting from an interpolated coarse grid result. Subsequently, a second simulation is performed for a period of $TU_\infty/\delta = 220$ inertial time units to gather statistics. For case A1, the skin friction statistics varied by a factor of 0.05% for the last 100 time units, which is an indication of well converged statistics.

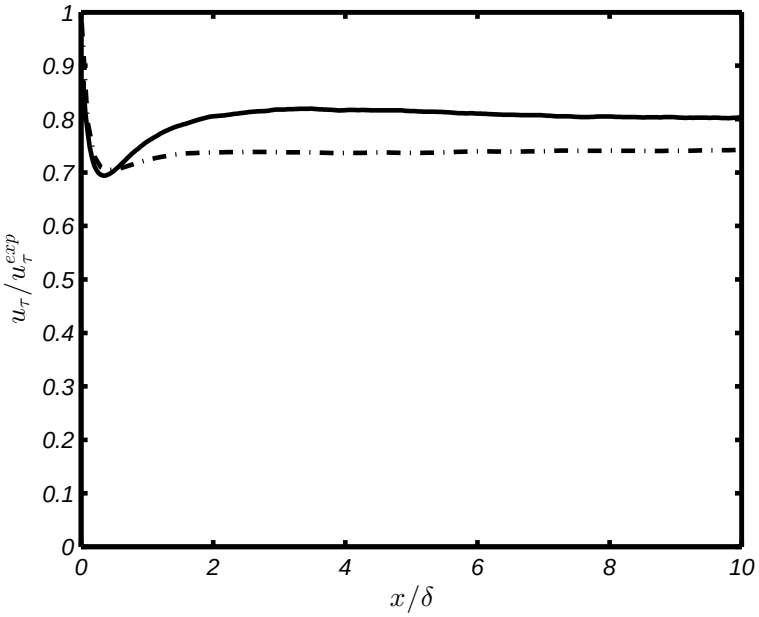

(a) Fine grid results (case A1), ratio of simulated friction velocity to experimental friction velocity. A ratio of one is equivalent to perfect match with the experiments. The solid line shows synthetic turbulence method, whereas dash-dotted shows the PIV-POD method. The synthetic method uses an integral length scale in the inflow plane of $L_z^i/\delta = 0.2$ and a streamwise integral time scale of $T_x^i U_\infty/\delta = 0.2$.

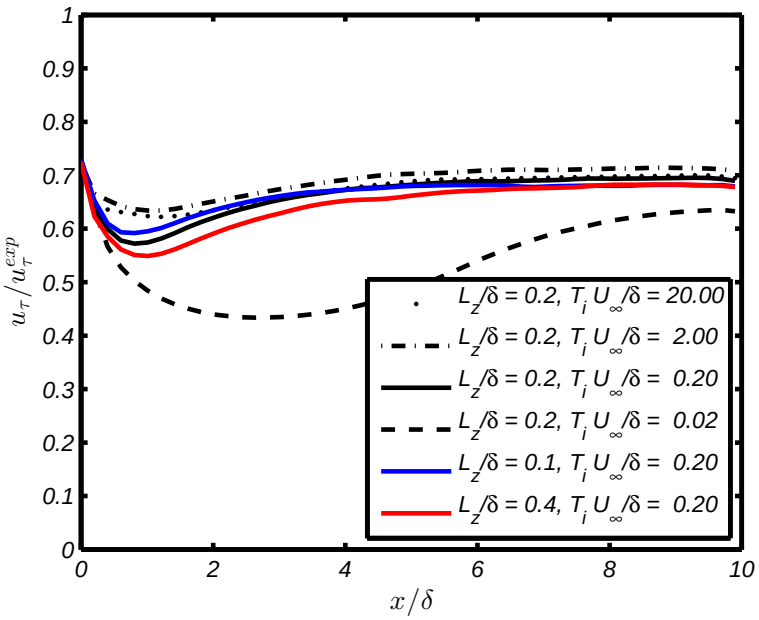

(b) Coarse grid results (case A2) for the synthetic turbulence method, showing the effect of changing the integral length scale in the inflow plane (L_z^i/δ) and the streamwise integral time scale ($T_x^i U_\infty/\delta$). The solid lines show the same integral time scale as in the fine grid case, but for varying integral length scales. The black dotted, dash-dotted and dashed lines show different integral time scales.

Figure 4.1 *Downstream development of scaled friction velocity u_τ/u_τ^{exp} where $u_\tau^{exp} = 0.35\ ms^{-1}$ is the friction velocity obtained in the experiments.*

Figure 4.1a shows the downstream development of the friction velocity scaled with the value obtained in the experiments. The solid black line shows the synthetic inflow results. In the upstream part of the domain, until approximately $x/\delta \approx 3$, there is a adaptation region, where the friction velocity drops and then recovers. From $x/\delta \approx 3$ there is a gradual decrease until the end of the domain. The dash-dotted black line shows the corresponding results using the method of Wingstedt *et al.* (2013). The synthetic inflow method underestimates the friction velocity by 19%, whereas the method of Wingstedt *et al.* (2013) underestimates the friction velocity by 25%, although requiring a shorter adaptation distance than the filtering method. The overall picture is that both methods perform well, with short adaptation lengths.

Ideally, the computed friction velocity should match the results of the experiments. However, it is not uncommon for LES models without wall functions in general, and for the dynamic Smagorinsky model in particular, to underestimate the skin friction (Piomelli *et al.*, 1988; Haertel & Kleiser, 1998). This is an effect that is expected to be diminished with increasing grid resolution. Indeed, our own simulations of periodic channel flows at $Re_\tau = 180$ and $Re_\tau = 395$, where the problem of inflow generation is absent, reveal that the skin friction coefficient does converge slowly towards DNS results upon grid refinement. However, even at the fine resolution of $\Delta x^+ = 30$ and $\Delta z^+ = 8$ there is a 6% underestimation of the friction velocity using the dynamic Smagorinsky model.

In Figure 4.1b, the effect of choosing different integral length and time scales on the obtained friction velocities is shown for a the coarse grid (case A2). The figure shows that for the same inflow parameters as for the fine grid (black solid line), the friction velocity is substantially lower. This is as expected from the previous discussion; fine resolution is needed to obtain a good estimate of the skin friction. The black dash-dotted and the black dotted lines show the resulting friction velocities when keeping the integral length scale, while increasing the integral time scale by a factor of ten and hundred, respectively. As can be seen, choosing a larger time scale results in a slight improvement in the adaptation region ($x/\delta < 3$). However, further downstream the results are quite similar. On the other hand, if the integral time scale is chosen as small as $T_x^i U_\infty/\delta = 0.02$ (see black dashed line), there is a clear reduction in performance compared to the others. Note that this choice of integral time scale for all practical reasons is equivalent no time correlation, since the time scale in this case is close to the time step in the simulation. The blue and the red solid lines show the effect of retaining the integral time scale at $T_x^i U_\infty/\delta = 0.2$, while modifying the integral length scale. The blue line shows the result for a reduction of a factor of two compared to $L_z^i/\delta = 0.2$, whereas the red line shows the result when doubling the length scale. Interestingly, a doubling of the length scale results in decreased performance, whereas reducing the length scale results in increased performance. This is contrary to the recommendations of Keating *et al.* (2004), who advocated the importance of retaining the largest scales. These results shows that the flow response is not very sensitive to the exact choice of integral time and length scales in the synthetic turbulence method. However, one should avoid choosing too small integral time scales. The same may be true also for integral length scales, but this limit has not been tested in the present work.

Vertical profiles of the mean velocity and Reynolds stresses at $x/\delta = 6$ are shown in Figure 4.2. Solid lines are simulated results using the synthetic digital filter inflow, dash dotted lines are simulated results from the POD-LSE method of Wingstedt *et al.* (2013), and squares are measured results from the wind tunnel. In Figure 4.2a, the mean velocity scaled by the freestream velocity is plotted as a function of wall distance. Both the synthetic digital filter inflow method and the POD-LSE method are in good agreement with the experiment. Close to the wall (see inset in Figure 4.2a), both methods yield lower velocities than the measurements. This difference is

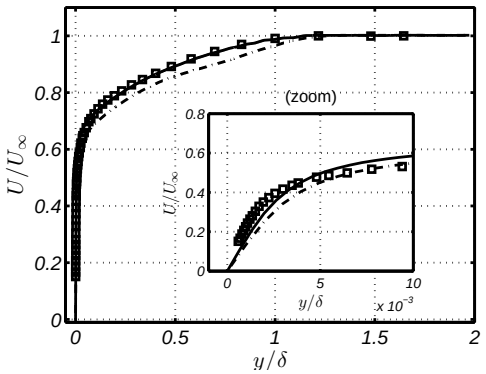

(a) Mean streamwise velocity U/U_∞ scaled in outer units.

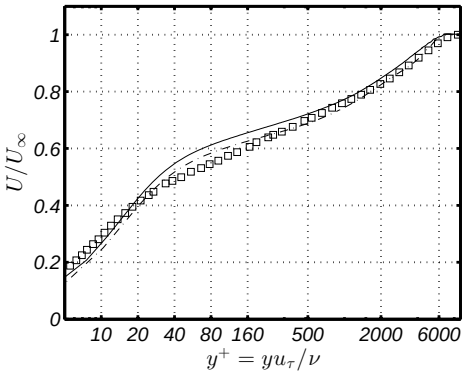

(b) Mean streamwise velocity, vertical coordinate scaled in viscous units.

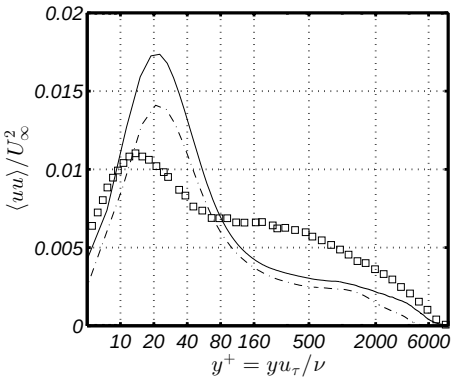

(c) Streamwise Reynolds stress, vertical coordinate scaled in viscous units

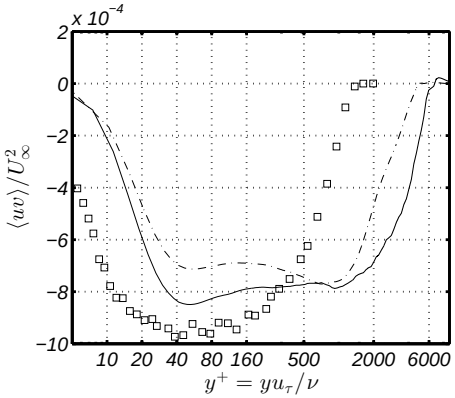

(d) Reynolds shear stress, vertical coordinate scaled in viscous units

Figure 4.2 *Simulated and experimental vertical profiles. Solid lines are synthetic digital filter inflow, dash-dotted lines are POD-LSE method of Wingstedt* et al. *(2013), and squares are experimental results.*

reflected in the friction velocities shown in Figure 4.1a, where both methods yielded lower friction velocities than the experiments. From the inset it can be seen that the region of discrepancy is extremely close to the wall. To better reveal near-wall features, a logarithmic scale is introduced in the wall normal distance. In addition the vertical coordinate is scaled in viscous units to simplify comparison with published results. The region $20 < yu_\tau/\nu < 1000$ is traditionally termed the log region. Figure 4.2b shows that the largest discrepancy between simulations and experiments occur in the lower part of the log region. In Figure 4.2c, the streamwise Reynolds stress $\langle uu \rangle / U_\infty^2$ is shown. The experiments yield a peak at $yu_\tau/\nu = 14$, in close agreement with DeGraaff & Eaton (2000), whereas both simulations yield $yu_\tau/\nu = 21$, which clearly is too far from the wall. This discrepancy is partly attributed to the underprediction of the skin friction. In addition, the amplitudes from both simulations are too large. This is a consequence of the excess of production by shear to turbulent dissipation. In the synthetic inflow simulation, the production to dissipation ratio is $\mathcal{P}/\varepsilon \approx 4$ in the log region. Typical DNS results yield a ratio of approximately unity, and the discrepancy shows one limitation of the dynamic Smagorinsky model (or similar eddy viscosity type of sub-grid stress models); the rate of turbulent dissipation is underestimated. In Figure 4.2c, one can observe a plateau in the streamwise Reynolds, located in the region $y^+ = 100$ to $y^+ = 500$, in the experiments. The location and magnitude of the plateau is in close agreement with the DNS results of Lozano-Durán & Jiménez (2014). The plateau is also present in both simulations, but the region is displaced compared to the experiments. The outer plateau is a footprint of the high Reynolds number, and is linked to the presence of very large-scale motions (VLSM), a concept that has received considerable attention during the last decade (Smits *et al.*, 2011). Hutchins & Marusic (2007) found structures in the log layer with lengths of $\sim 20\delta$ able to interact with the near wall region, leading to an increase in near wall peak turbulence intensity. In Figure 4.2d, the Reynolds shear stress $\langle uv \rangle / U_\infty^2$ is shown. Observe that the magnitude of the simulated Reynolds shear stresses are lower than the experiments. There is also a discrepancy in the location, which can not be explained by the difference in friction velocity. By closer examination of the experimental Reynolds shear stress, two features are observed. Firstly, the experimental profile underestimates the stress relation $\langle uv \rangle / u_\tau^2 \approx 1$ in the log region (Tennekes & Lumley, 1972). Secondly, the magnitude drops suspiciously slow towards the wall. These factors may indicate that the measured Reynolds shear stress is not of sufficient quality. The behaviour of the Reynolds shear stress in both simulations seems reasonable and in close agreement with the constant stress relation, as well as experimental results of DeGraaff & Eaton (2000) and DNS results of Sillero *et al.* (2013). The historical focus on low Reynolds turbulence, which until now made sense due to computational capacity limitations, has often been justified based on the observation that the peak production occurs at approximately $y^+ = 12$. While this is true for low Reynolds numbers, it does not hold for high Reynolds number turbulence. Instead, for high Reynolds number turbulence, production is active in the entire log region. The main contribution to the production of turbulence energy in boundary layers is $\langle uv \rangle \partial_y U$. Therefore, in order to achieve non-zero production throughout the log region, nonzero Reynolds shear stresses are required in the entire log region. From the figure it is seen that this is clearly true for the present simulations and the simulations in Wingstedt *et al.* (2013), and may be taken as evidence that important features of high Reynolds number turbulent boundary layer flow are reproduced in the simulations.

4.2 Recreating the flow in the EnFlo tunnel

To reproduce the boundary layer flow from the EnFlo tunnel described in Section 2.2, two cases have been simulated. In the wind tunnel, the flow is subject to the combined effects of the turbulent air produced by the fan, the vortex generators, and the obstacles on the floor. To isolate the effect of the roughness obstacles, both a smooth wall boundary and a rough wall boundary layer flow have been simulated, and in both cases, synthetic inflow conditions were used at the upstream boundary. In the synthetic method, the two main input parameters (apart from mean velocity profiles and Reynolds stresses) are the integral length scales in the inflow plane and the integral time scale in the streamwise direction. The integral length scales were set so as to define a series of piecewise constant profiles with parameters derived from the experiments (see Table 4.1). Building on the hypothesis of Keating *et al.* (2004), that the large scales are the most important to retain, a simulation with uniform integral length and time scale of $L_z^i = 0.6$ and $T_x^i = 0.6$ was also performed. For the present case, although the statistics far downstream agree well between the two cases, the adaptation region was shorter when using varying length and time scales.

Table 4.1 *Setup of integral length and time scales for the EnFlo simulations. The integral length scale is set to piecewise constant in intervals ranging from y_0/δ to y_1/δ.*

y_0/δ	y_1/δ	L_z^i/δ	$T_x^i U_\infty/\delta$
0	0.05	0.15	0.3
0.05	0.1	0.25	0.42
0.1	0.4	0.45	0.56
0.4	0.9	0.3	0.33
0.9	1.5	0.2	0.2

The numerical grid was created to ensure high resolution close to the wall using one to three splits in the wall-normal direction as seen in Figure 4.3 a) and b). Figure 4.3 a) shows a two-dimensional view of a subset of the domain. Between the wall and $y = 0.02\delta$, corresponding to a viscous length of $y^+ \approx 70$, the grid spacing is $(\Delta x, \Delta y, \Delta z) = (4.4, 2.0, 4.4) \times 10^{-3}\delta$, corresponding to $(\Delta x^+, \Delta y^+, \Delta z^+) = (16, 7, 16)$ viscous lengths. In the domain $y = 0.02\delta$ to $y = 0.51\delta$, the grid spacing is uniform with a value of 0.013δ, corresponding to 47 viscous lengths. In the upper domain the uniform grid spacing is 0.039δ, corresponding to 144 viscous lengths. In Figure 4.3 b), the one to three splitting of the grid, which takes place at $y = 0.02\delta$ and $y = 0.51\delta$ is illustrated. The total dimensions of the grid are $L_x \times L_y \times L_z = 8\delta \times 1.5\delta \times 3.5\delta$, with a total of 13 million grid points. The roughness boundary layer flow is generated by means of thin plates of height $h_r = 0.02\delta$, placed onto the floor in the region $0 < x/\delta < 5$, with a downstream spacing of 0.12δ (see Figure 2.3). This configuration matches geometrically the set-up in the wind tunnel. Both the smooth wall boundary layer flow and the rough wall boundary layer flow were simulated in two stages. Initially, to establish statistically stationary conditions, a simulation was run for $TU_\infty/\delta \approx 130$ inertial time units. Thereafter, statistics were gathered for another $TU_\infty/\delta \approx 160$ inertial time units.

Vertical profiles of the mean streamwise velocity, streamwise Reynolds stress, and Reynolds shear stress are shown in Figure 4.4. The thin solid lines represent synthetic turbulence inflow

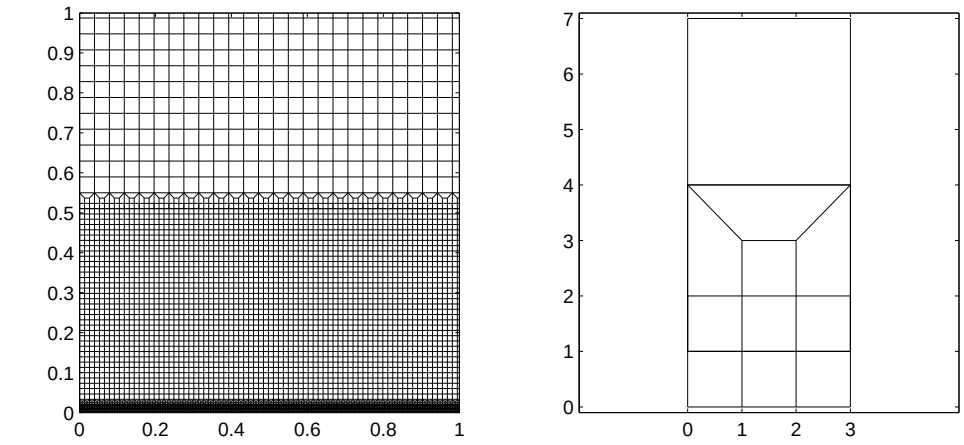

Figure 4.3 *a) Two-dimensional view of the grid for a portion of the grid. b) Schematic view of the grid splitting that ensures higher resolution close to the wall and a step-wise coarsening towards the top of the boundary layer.*

over a smooth wall, the dash dotted lines represent synthetic turbulence inflow over a rough wall, whereas the squares represent experimental results. From Figure 4.4a it is seen that in the outer part of the boundary layer ($z/\delta > 0.3$), both simulations yield similar mean flow profiles, in close agreement with experiments. This indicates, as would be expected, that in the outer part of the boundary layer, advection by the mean flow is the dominant mechanism. Closer to the wall, the rough wall case is clearly in better agreement with the experiments than the smooth wall case. In order to assess the quality of the smooth-wall simulation, the friction velocity is compared to the flat-plate boundary-layer flow experiments of DeGraaff & Eaton (2000). Indeed, the friction velocity derived from the gradient of the mean flow (i.e. from the wall shear stress) at the wall, $u_\tau/U_\infty = \sqrt{\nu \partial_y U|_{y=0}}/U_\infty = 0.038$, is in close agreement with the flat plate experimental results of DeGraaff & Eaton (2000). Below $z/\delta \sim 0.005$, the mean flow, and therefore also the wall shear stress, of the smooth and the rough wall case (see inset of Figure 4.4a), are almost identical. In the experiments, the friction velocity is estimated as the square root of the mean Reynolds shear stress in the lower 20% of the boundary layer ($z/\delta < 0.2$), with a resulting value of $u_\tau/U_\infty = 0.055$. Figure 4.4c shows that whereas the rough wall case has a shear stress magnitude comparable to the experiments, the smooth wall case underestimates the magnitude significantly. Indeed, using the Reynolds shear stress to define the friction velocity, it is found that $u_\tau/U_\infty = 0.037$ for the smooth wall case and $u_\tau/U_\infty = 0.051$ for the rough wall case, which is clearly in better agreement with the experiments. It is interesting to note that in the smooth wall case, the two ways of defining the characteristic velocity scale are almost identical, which confirms that there is a constant stress layer, as expected for a flat plate boundary layer flow. On the contrary, for the roughness boundary layer flow, the friction velocities based on wall shear stress is significantly lower than the one based on Reynolds shear stress. Hence, the most important contribution to turbulent mixing stems from the pressure drag created by the upstream obstacles in the rough wall case.

Also in terms of streamwise Reynolds stresses, the rough wall case is in better agreement with experiments than the smooth wall. Interestingly, the near-wall behaviour ($z/\delta < 0.01$) is again very similar for the two simulations. The smooth wall case has a single peak in the streamwise Reynolds

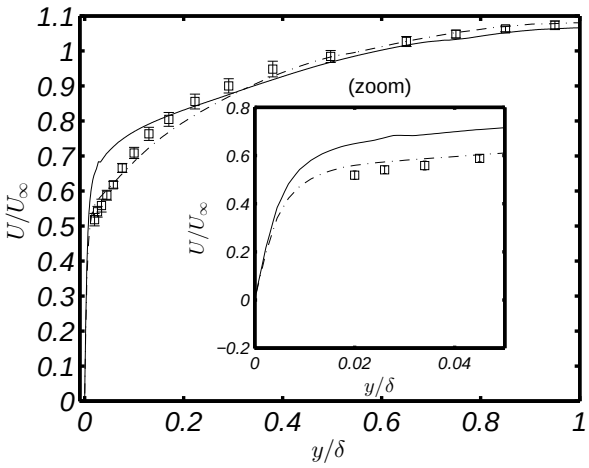

(a) Mean streamwise velocity U/U_∞

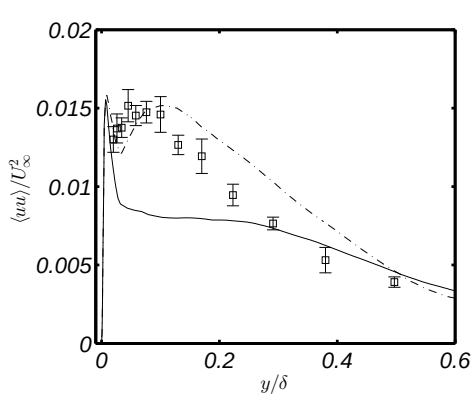

(b) Streamwise Reynolds stress $\langle uu \rangle / U_\infty^2$

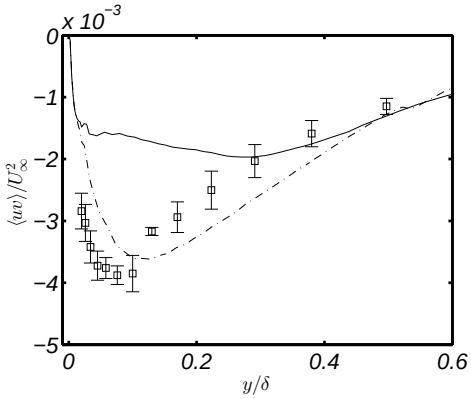

(c) Reynolds shear stress $\langle uv \rangle / U_\infty^2$

Figure 4.4 *Simulated and experimental vertical profiles. Solid lines are smooth wall synthetic inflow, dash-dotted lines are rough wall synthetic inflow, and squares are experimental results.*

stress, located slightly below $z/\delta = 0.015$ (about 20 wall units). The rough wall case on the other hand, has a double peak behaviour, with the first peak being almost identical to the smooth wall case, both in location and magnitude, and the second peak located at $z/\delta = 0.1$. The inner peak is related to viscous mechanisms, whereas the outer peak is related to turbulence produced by the aerodynamic drag of the obstacles.

To conclude, even at the relatively small roughness Reynolds number in the present case, it is necessary to include the geometric effects of the roughness elements in the wind tunnel in order to reproduce the flow numerically. Although the smooth wall simulation fails to provide a good representation of the wind tunnel results, it is seen to be in good agreement with flat plate experiments. This may be taken as evidence of the satisfactory performance of the synthetic turbulence generator and the Large Eddy Simulation code.

5 Conclusions

In this report, Large Eddy Simulation of two high Reynolds number turbulent boundary layer flows, where measurements are available for comparison, has been performed. The motivation for the study is twofold. First, to check the performance of our Large Eddy Simulation code as a tool to study wall bounded flows. Second, to assess the quality of the synthetic inflow generator which is implemented in the code. Indeed, one key issue to address when performing high fidelity techniques such as Direct Numerical or Large Eddy Simulation for turbulent boundary layers, is the need to introduce artificial time dependent boundary conditions at the upstream edge of the computational domain. Since one is limited by available computational resources, it is of interest to reduce the size of the domain considered as much as possible. To achieve this one needs to prescribe the behaviour of the flow at the inlet. In this report, we have considered the use of a digital filter based synthetic turbulence generator, where the mean velocity and Reynolds stress profiles are prescribed at the inflow. Based on this information together with estimates of length and time scales in the flow, a time varying "synthetic" turbulence field is generated by manipulation of random noise. Naturally, these type of methods produce unphysical results some distance downstream of the inlet, and one main interest is to evaluate the length of the adaptation region. Another issue is related to how well the simulated turbulent flows perform in terms of comparison with realistic flows.

The first flow studied is a high Reynolds turbulent boundary layer flow with a slight favourable pressure gradient. We find that there is a downstream adaptation region of approximately three boundary layer thicknesses. Previously, adaptation lengths of approximately 20 boundary layer thicknesses have been reported (Klein *et al.*, 2003; di Mare *et al.*, 2006; Keating *et al.*, 2004), but those results have typically been for lower Reynolds numbers, where the intrinsic instability mechanisms are weaker. It is interesting to note that the method of Wingstedt *et al.* (2013) has an adjustment region of only two boundary layer thicknesses, which is impressive. However, in that method the friction velocity stabilises at a lower level than in the synthetic turbulence method. In terms of Reynolds stresses the two methods perform similarly. Given the similar behaviour of the two methods and that the synthetic turbulence method requires less input data, the synthetic turbulence would be the method of choice for general flow situations where limited knowledge is available.

The second flow studied is a boundary layer flow over a rough wall. In the experiment, the incoming turbulent flow is produced by the combined effect of a fan and large scale vortex generators. As the flow enters the test section, it interacts with small obstacles at the floor, to create a boundary layer flow that is reminiscent of that in the atmospheric boundary layer. To isolate the effect of the wall obstacles, two simulations are performed, both of which use synthetic inflow turbulence imposed at the upstream boundary. In the first simulation, a smooth lower wall is used, whereas in the second simulation a rough lower wall, matching geometrically the set up in the experiment, is used. The rough wall simulation is in excellent agreement with the experiment, clearly outperforming the smooth wall simulation. This shows that the dynamical relevance of the obstacles at the lower wall is significant. Although the smooth wall simulation provide flow profiles that are in poor agreement with the experimental results, the flow adapts fairly quickly (within four boundary layer thicknesses) to a well behaved smooth wall turbulent boundary layer flow, in close agreement with published smooth wall results. The digital filter synthetic inflow

generator is therefore seen to perform well as a tool to introduce artificial turbulent flow fields at the upstream boundary.

Large Eddy Simulation of turbulent boundary layer flows is a challenging task due to strict resolution requirements close to the wall, where the flow is dominated by viscous mechanisms. Therefore, in order to obtain a good measure of the skin friction, high resolution is needed. On the other hand, the large scale structures, present only in high Reynolds number flows, are well reproduced in the simulations, even at relatively coarse resolution.

Acknowledgements

This work was funded by the Norwegian Research Council (NFR) RENERGI programme, grant number KPN-216465, “Fluid Structure Interactions for Wind Turbines” (FSI-WT) and by the European Defence Agency (EDA) project B-1097-ESM4-GP “Modelling the dispersion of toxic industrial chemicals in urban environments” (MODITIC). Some simulations were performed on the computational resources at NTNU provided by NOTUR, www.sigma2.no. The rough wall simulation was performed by Daniel Eriksson.

Bibliography

Batten, P., Goldberg, U. & Chakravarthy, S. 2004 Interfacing Statistical Turbulence Closures With Large-Eddy Simulation. *AIAA journal* **42** (3), 485–492.

Bonnet, J.P., Cole, D.R., Delville, J., Glauser, M.N. & Ukeiley, L.S. 1994 Stochastic Estimation and Proper Orthogonal Decomposition: Complementary Techniques for Identifying Structure. *Exp. Fluids* **17** (5), 307–314.

DeGraaff, D. B. & Eaton, J. K. 2000 Reynolds Number Scaling of The Flat-Plate Turbulent Boundary Layer. *J. Fluid Mech.* **422**, 319–346.

Delville, J., Braud, P., Coudert, S., Foucaut, J.-M., Fourment, C., George, W. K., Johansson, P. B. V., Kostas, J., Mehdi, F., Royer, A., Stanislas, M. & Tutkun, M. 2009 The WALL-TURB Joined Experiment To Assess The Large Scale Structures In A High Reynolds Number Turbulent Boundary Layer. In *Progress In Wall Turbulence: Understanding and Modelling* (ed. M. Stanislas, J. Jimenez & I. Marusic).

Druault, P., Lardeau, S., Bonnet, J.-P., Coiffet, F., Delville, J., Lamballais, E., Largeau, J.-F. & Perret, L. 2004 Generation of Three-Dimensional Turbulent Inlet Conditions for Large-Eddy Simulation. *AIAA J.* **42** (3), 447–456.

Ferrante, A. & Elghobashi, S. E. 2004 A Robust Method for Generating Inflow Conditions for Direct Numerical Simulations of Spatially-Developing Turbulent Boundary Layers. *J. Comp Phys.* **198**, 372–287.

Fossum, H. 2015 Computational Modeling of Stably Stratified, Turbulent Shear Flows. PhD thesis, Department of Mathematics, University of Oslo.

Haertel, C. & Kleiser, L. 1998 Analysis and Modelling of Subgrid-Scale Motions in Near-Wall Turbulence. *J. Fluid Mech.* **356**, 327–352.

Ham, F. & Iaccarino, G. 2004 Energy Conservation In Collocated Discretization Schemes on Unstructured Meshes. *Annual Research Briefs* **2004**, 3–14.

Ham, F., Mattsson, K. & Iaccarino, G. 2006 Accurate and Stable Finite Volume Operators For Unstructured Flow Solvers. *Tech. Rep.*. Center For Turbulence Research (CTR).

Hutchins, N. & Marusic, I. 2007 Evidence of Very Long Meandering Features in the Logarithmic Region of Turbulent Boundary Layers. *J. Fluid Mech.* **579**, 1–28.

Ikeda, T. & Durbin, P. A. 2007 Direct Simulations of Rough-Wall Channel Flow. *J. Fluid Mech.* **571**, 235–263.

Jarrin, N., Benhamadouche, S., Laurence, D. & Prosser, R. 2006 A Synthetic-Eddy-Method For Generating Inflow Conditions For Large-Eddy Simulations. *Int. J. Heat Fluid* **27** (4), 585–593.

Keating, A., Piomelli, U., Balaras, E. & Kaltenbach, H.-J. 2004 A Priori and A Posteriori Tests of Inflow Conditions For Large-Eddy Simulation. *Phys. Fluids* **16**, 4696.

KLEIN, M., SADIKI, A. & JANICKA, J. 2003 A Digital Filter Based Generation of Inflow Data For Spatially Developing Direct Numerical or Large Eddy Simulations. *J. Comp Phys.* **186** (2), 652–665.

KUNDU, P. K., COHEN, I. M. & DOWLING, D. R. 2012 *Fluid Mechanics*, 5th edn. Elsevier Academic Press.

LE, H., MOIN, P. & KIM, J. 1997 Direct Numerical Simulation of Turbulent Flow Over A Backward-Facing Step. *J. Fluid Mech.* **330**, 349–374.

LI, N., BALARAS, E. & PIOMELLI, U. 2000 Inflow Conditions For Large-Eddy Simulations of Mixing Layers. *Phys. Fluids* **12**, 935.

LOZANO-DURÁN, ADRIÁN & JIMÉNEZ, JAVIER 2014 Effect of the computational domain on direct simulations of turbulent channels up to re τ= 4200. *Phys. Fluids* **26**, 011702.

LUND, T. S, WU, X. & SQUIRES, K. D. 1998 Generation of Turbulent Inflow Data For Spatially-Developing Boundary Layer Simulations. *J. Comp Phys.* **140** (2), 233–258.

MAHESH, K., CONSTANTINESCU, G., APTE, S., IACCARINO, G., HAM, F. & MOIN, P. 2002 Progress Toward Large-Eddy Simulation of Turbulent Reacting and Non-Reacting Flows In Complex Geometries. *Annual Research Briefs* pp. 115–142.

MAHESH, K., CONSTANTINESCU, G. & MOIN, P. 2004 A Numerical Method For Large-Eddy Simulation In Complex Geometries. *J. Comp Phys.* **197**, 215–240.

DI MARE, L, KLEIN, M, JONES, WP & JANICKA, J 2006 Synthetic Turbulence Inflow Conditions for Large-Eddy Simulation. *Phys. Fluids* **18**, 025107.

PERRET, L., DELVILLE, J., MANCEAU, R. & BONNET, J.-P. 2008 Turbulent Inflow Conditions For Large-Eddy Simulation Based On Low-Order Empirical Model. *Phys. Fluids* **20**, 075107.

PIOMELLI, U., FERZIGER, J. & MOIN, P. 1988 Model Consistency in Large Eddy Simulation of Turbulent Channel Flows. *Phys. Fluids* **31**, 1884.

POPE, S. B. 2000 *Turbulent Flows*. Cambridge, United Kingdom: Cambridge University Press.

RASHID, F., VARTDAL, M. & GRUE, J. 2011 Oscillating Cylinder In Viscous Fluid: Calculation of Flow Patterns and Forces. *J. Eng. Math.* **70** (1-3), 281–295.

REYNOLDS, O. 1895 On the Dynamical Theory of Incompressible Viscous Fluids and the Determination of the Criterion. *Phil. Trans. R. Soc. A.* **168**, 123–164.

SAGAUT, P. 2006 *Large Eddy Simulation For Incompressible Flows: An Introduction*, 3rd edn. Springer.

SILLERO, JUAN A, JIMÉNEZ, JAVIER & MOSER, ROBERT D 2013 One-point statistics for turbulent wall-bounded flows at reynolds numbers up to $\delta^+ \approx 2000$. *Phys. Fluids* **25**, 105102.

SMITS, A. J., MCKEON, B. J. & MARUSIC, I. 2011 High-Reynolds Number Wall Turbulence. *Annu. Rev. Fluid Mech.* **43**, 353–375.

SPALART, P. R. 1986 Numerical Study of Sink-Flow Boundary Layers. *J. Fluid Mech.* **172**, 307–328.

Spalart, P. R. 1988 Direct Simulation of A Turbulent Boundary Layer Up To Re_θ= 1410. *J. Fluid Mech.* **187**, 61–98.

Spalart, P. R. & Leonard, A. 1985 Direct Numerical Simulation of Equilibrium Turbulent Boundary Layers. In *5th Symposium on Turbulent Shear Flows*, , vol. 1, p. 9.

Spille-Kohoff, A. & Kaltenbach, H.-J. 2001 Generation of Turbulent Inflow Data With A Prescribed Shear-Stress Profile. *Tech. Rep.*. DTIC Document.

Stanislas, M., Foucaut, J.-M., Coudert, S., Tutkun, M., George, W. K. & Delville, J. 2009*a* Calibration of The WALLTURB Experiment Hot Wire Rake With Help of PIV. In *Progress In Wall Turbulence: Understanding and Modelling* (ed. M. Stanislas, J. Jimenez & I. Marusic).

Stanislas, M., Jimenez, J. & Marusic, I., ed. 2009*b* *Progress In Wall Turbulence: Understanding and Modelling*. Springer.

Tennekes, H. & Lumley, J. L. 1972 *A First Course in Turbulence*. MIT Press.

Tutkun, M. 2008 Structure of Zero Pressure Gradient High Reynolds Number Turbulent Boundary Layers. PhD thesis, Division of Fluid Mech., Dept. App. Mech., Chalmers University of Technology.

Vartdal, M. 2016 Computing Turbulence Structure Tensors in Plane Channel Flow. *Computers & Fluids* **136**, 207–211.

Vik, T., Tørnes, J. A. & Reif, B. A. P. 2015 Simulations of the Release and Dispersion of Chlorine and Comparison with the Jack Rabbit Field Trials. *Tech. Rep.* 01474. FFI, Norwegian Defence Research Establishment.

Wingstedt, E. M. M., Osnes, A. N., Åkervik, E., Eriksson, D. & Reif, B. A. P. 2016 Large-Eddy Simulation of Dense Gas Dispersion Over A Simplified Urban Area. *Atm Env* **251**, 605–616.

Wingstedt, E. M. M., Vartdal, M., Osnes, A. N. & Tutkun, M. 2013 Development of LES Inflow Conditions For Turbulent Boundary Layers. *Tech. Rep.* 02420. FFI, Norwegian Defence Research Establishment.

About FFI

The Norwegian Defence Research Establishment (FFI) was founded 11th of April 1946. It is organised as an administrative agency subordinate to the Ministry of Defence.

FFI's MISSION

FFI is the prime institution responsible for defence related research in Norway. Its principal mission is to carry out research and development to meet the requirements of the Armed Forces. FFI has the role of chief adviser to the political and military leadership. In particular, the institute shall focus on aspects of the development in science and technology that can influence our security policy or defence planning.

FFI's VISION

FFI turns knowledge and ideas into an efficient defence.

FFI's CHARACTERISTICS

Creative, daring, broad-minded and responsible.

Om FFI

Forsvarets forskningsinstitutt ble etablert 11. april 1946. Instituttet er organisert som et forvaltningsorgan med særskilte fullmakter underlagt Forsvarsdepartementet.

FFIs FORMÅL

Forsvarets forskningsinstitutt er Forsvarets sentrale forskningsinstitusjon og har som formål å drive forskning og utvikling for Forsvarets behov. Videre er FFI rådgiver overfor Forsvarets strategiske ledelse. Spesielt skal instituttet følge opp trekk ved vitenskapelig og militærteknisk utvikling som kan påvirke forutsetningene for sikkerhetspolitikken eller forsvarsplanleggingen.

FFIs VISJON

FFI gjør kunnskap og ideer til et effektivt forsvar.

FFIs VERDIER

Skapende, drivende, vidsynt og ansvarlig.

FFI's organisation

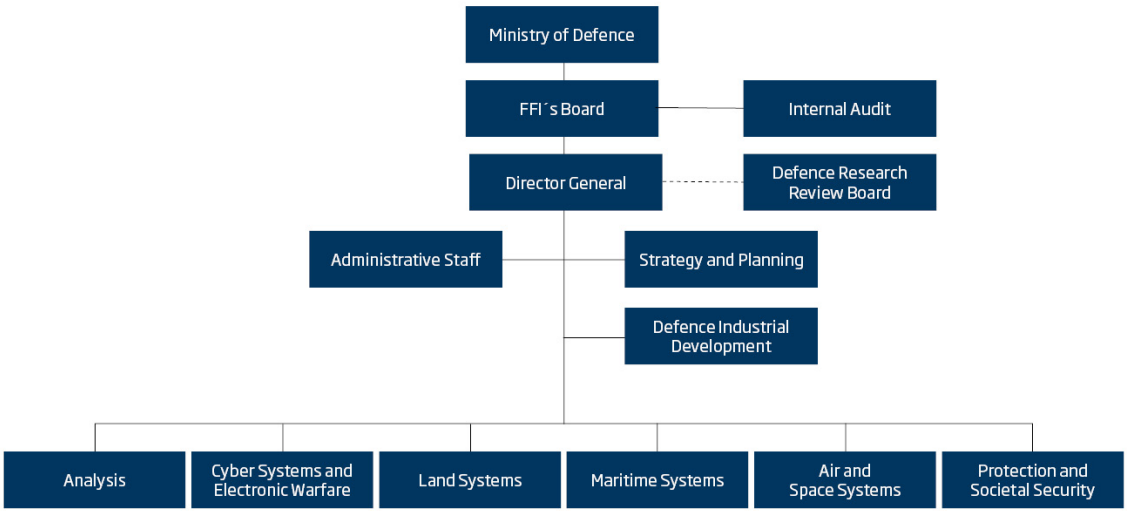

Forsvarets forskningsinstitutt
Postboks 25
2027 Kjeller

Besøksadresse:
Instituttveien 20
2007 Kjeller

Telefon: 63 80 70 00
Telefaks: 63 80 71 15
Epost: ffi@ffi.no

Norwegian Defence Research Establishment (FFI)
P.O. Box 25
NO-2027 Kjeller

Office address:
Instituttveien 20
N-2007 Kjeller

Telephone: +47 63 80 70 00
Telefax: +47 63 80 71 15
Email: ffi@ffi.no

FFI Forsvarets forskningsinstitutt
Norwegian Defence Research Establishment